Intriguing Structures and Magic Sizes of Heavy Noble Metal Nanoclusters around Size 55 governed by Relativistic Effect and Covalent Bonding

X.J. Zhao,[1] X.L. Xue,[1] Z.X. Guo,[2,1] Yu Jia,[1] S.F. Li,[1,3,a)] Zhenyu Zhang,[3,4,b)] and Y.F. Gao[5,6,c)]

[1]*International Laboratory for Quantum Functional Materials of Henan and School of Physics and Engineering, Zhengzhou University, Zhengzhou, 450001, China*

[2]*Department of Chemistry and London Centre for Nanotechnology, University College London, London WC1H, UK*

[3]*ICQD, Hefei National Laboratory for Physical Sciences at the Microscale, University of Science and Technology of China, Hefei, Anhui 230026, China*

[4]*Synergetic Innovation Center of Quantum Information and Quantum Physics, University of Science and Technology of China, Hefei, Anhui 230026, China*

[5]*Department of Materials Science and Engineering, University of Tennessee, Knoxville, TN 37996, USA*

[6]*Materials Science and Technology Division, Oak Ridge National Laboratory, Oak Ridge, TN 37831, USA*

Abstract

Nanoclusters usually display exotic physical and chemical properties due to their intriguing geometric structures in contrast to their bulk counterparts. By means of first-principles calculations within density functional theory, we find that heavy noble metal Pt_N nanoclusters around the size N=55 prefer an open configuration, rather than previously reported close-packed icosahedron or core-shell structures. Particularly, for Pt_N, the widely supposed icosahedronal magic cluster, is changed to a three-atomic-layered structure with D_{6h} symmetry, which can be well addressed by our recently established generalized Wulff construction principle (GWCP). However, the magic number of Pt_N clusters around 55 is shifted to a new odd number of 57. The high symmetric three-layered Pt_{57} motif is mainly stabilized by the enhanced covalent bonding contributed by both spin-orbital coupling effect and the open *d* orbital ($5d^9 6s^1$) of Pt, which result in a delicate balance between the enhanced Pt-Pt covalent bonding of the interlayers and negligible *d* dangling bonds on the cluster edges. These findings about Pt_N clusters are also applicable to Ir_N clusters, but qualitatively different from their earlier neighboring element Os and their later neighboring element Au. The magic numbers for Os and Au are even, being 56 and 58 respectively. The findings of the new odd magic number 57 is an important supplementary of the recently established GWCP.

I. Introduction

Because of their intriguing geometric structures and their atomic scales that promote the quantum size effects, nanoclusters have drastically different physical and chemical properties than their bulk counterparts, and thus leading to many unique applications.[1-4] Interestingly, these nanoclusters are energetically more stable at certain sizes and referred as magic clusters[5-8]. Clearly, the understanding of this "magic size" phenomenon will help us tune their individual physical/chemical properties, and also possibly use them as building blocks to assemble into novel materials that have unprecedented functionalities.[2,9-11]

Three mechanisms have been successfully identified for the magic-size behavior of a given nanocluster, including: the atomic shell closure[5] model for inert gas clusters; electronic shell closure[6] mechanism for simple metal clusters; and the recently established generalized Wulff construction principle (GWCP)[12] for transition metal clusters. The atomic shell closure model is a geometric construction principle that predicts the formation of icosahedral clusters/structures at magic sizes of 13, 55, 147, etc. The new mechanism GWCP[12] emphasizes the minimization of the total edge energy of a given transition metal nanocluster due to the excess energy arising from the undesirable *d*-type dangling bonds located on the cluster edges. Correspondingly, around size 55, the magic numbers of transition metal nanoclusters are predicted to be even, such as 56, rather than the widely accepted odd number 55 as predicted by the atomic shell closure model, which was strongly supported by recent experimental observations.[13,14] Since the edge energy is largely governed by the *d*-type dangling

bonds, the GWCP is applicable for almost all *nd* transition metal elements (*n*=3, 4, 5), with the only exceptions being the earliest and latest TM cases.[12] This exception can be attributed to the negligible numbers of *d*-type dangling bonds on the edge atoms for both the earliest and the latest TMs as compared to the central ones.[12]

We emphasize that in these aforementioned exceptions, the latest noble elements, such as Au, is particularly novel and intriguing, due to the relativistic effect[15-18] which stabilizes the *s* orbitals and destabilizes the *d* orbitals, leading to the enhanced *s*-*d* hybridizations. Correspondingly, Au_N nanoclusters exhibit the enhanced covalent bonding,[19,20] the preference of planar open structure in the small size regime (*N*=3~13),[16] exotic cage structures in a relatively larger regime (*N*=16~20),[21] symmetry breaking based amorphous structures[15] and even magic number of 58 due to both atomic and electronic shell closures around size 55, and size-selective catalysis for an even larger size regime.[22]

Then, one simple question naturally arises: does the relativistic effect also play the key role in determining the geometric structure, magic sizes, physical and chemical properties of Pt nanoclusters? First, as the nearest neighbor of Au in the periodic table, noble metal Pt is also a well-known catalyst[23-27] and may also possess strong relativistic effects as implied by the comparable relativistic contraction of the 6*s* shells between Pt and Au.[28] Additionally, the *d* orbital of Pt is of an open-shell configuration, which helps to form stronger *d*-*d* directional bonding for Pt nanostructures despite its relatively weaker relativistic effect than Au. However, the synergetic or competitive effects between the relativistic effect and the open-shelled *d* orbital on the geometric/electronic

structures of heavy noble nanoclusters, such as Pt_N, have not been rigorously established. Importantly, we will show later that Pt actually lies at the boundary of the elements whose atomic stacking rule and magic numbers of nanoclusters may not be guided simply by GWCP or the electronic and geometric shell-closure models.[5,6,8,12] Therefore, the atomic stacking rule and magic numbers of Pt_N are hard to specifically predict from the established principles. Despite recent studies on Pt_{13},[29,30] Pt_{55} nanoclusters,[12,31-35] and other TM_{55} nanoclusters[12,13] the above question still remains unclear and awaits for a definite answer in order to determine accurately the specific structures and properties of the nanoclusters consisting of "boundary" element Pt for practical applications such as nanocatalysis.

In this paper, by means of detailed first-principles calculations, we have specifically identified that Pt_N nanoclusters around size 55 prefer an intriguing three-layered stacking form, mainly due to the synergetic effect from the established GWCP, relativistic effect and the significant covalent bonding as well. Correspondingly, the magic cluster of Pt_N around size 55 is identified to be Pt_{57}, meanwhile, the magic cluster now is a highly symmetric (D_{6h}) three-layered-wheel (TLW) configuration, rather than the widely supposed I_h,[31,32] O_h,[33] or amorphous core-shell motifs.[34,35] The differences in atomic stacking and in magic numbers around 55 between Pt_N and Au_N are mainly due to a relatively stronger covalent bonding that results from the open-shell *d* orbital in the former case, as opposed to the closed-shell of the latter. The present findings are also valid up to Iridium. Additionally, when moving towards the central element Os with more unpaired *d* electrons as compared to Ir and Pt, the present TLW open

structures are found to be significantly less stable. Correspondingly, the established GWCP mechanism[12] must dominate, due to the critically undesirable *d*-type dangling bonds[12] located on the sharp edges of TLW structures on one hand, and due to the significantly reduced relativistic effect[28] on the other hand.

The remainder of the paper is organized as follows. The methodology is described in Sec. II. The results and discussion are presented in Sec. III. The main conclusions are summarized in Sec. IV.

II. Method

Our calculations adopted the density functional theory (DFT)[36] within the spin-polarized generalized gradient approximation (GGA)[37] as implemented in the VASP code.[38] The interaction of the valence electrons with the ionic core was described by the projector augmented wave (PAW) method[39] with PW91 form as the exchange-correlation functional. The wave functions are expanded in a plane wave basis with an energy cutoff of 230.277 eV. To identify the accuracy of our calculation method, we have carried out calculations on the properties of both Pt_2 molecule and Pt bulk crystal. The calculated vibrational frequency (215.613 cm^{-1}) of the Pt_2 molecule agrees well with experimental value[40] of 222.26 ± 0.31 cm^{-1}, and the calculated bond length (2.379 Å) of the Pt_2 is also very close to the experimental value of 2.333 Å.[41] In addition, for the fcc-Pt crystal, the optimized crystal constant 3.991 Å agree well with experimental value 3.92 Å.[42] The atomic positions of clusters were optimized in a big simple cubic cell with edge length of 25 Å and the energy convergence of 0.001 eV. To obtain the ground state configurations of the Pt clusters, we have considered many initial

candidate configurations manually constructed or computationally generated via high-temperature first-principles molecular dynamic (MD) simulations, and classical MD simulations performed by LAMMPS[43] code as well. We have also carried out structural optimizations by using the particle swarm optimization (CALYPSO) code,[44,45] which is very powerful for searching for low energy structures. In addition, the low-energy structural candidates obtained by recent works on TM_{55} clusters[12,34] have also been checked for Pt_{55} in this work. Finally, the most stable structures are further examined by thermal dynamic simulations in high temperature and vibrational property analysis.

III. Results

We start our systematic optimization of Pt_{55} structures first without considering the spin-orbital coupling effects, *i.e.*, by using the plain GGA calculations. In Figure 1, we summarize six representative low-energy Pt_{55} candidate structures optimized. The most stable Pt_{55} structure consists of an amorphous core-shell configuration with 9 core atoms and 46 shell atoms, which is denoted as C9-S46 in Fig. 1(a). This structure can be obtained by moving 4 inner Pt atoms from the core of an icosahedral (I_h) Pt_{55} structure to the surface shell, followed by further optimization. The resulting total energy is lower by 5.313 eV for the structure (a) than that of the perfect I_h structure (f). Note that, previously, Baletto, *et al.*,[31] and Apra, *et al.*,[32] reported that Pt_{55} prefers I_h structure, essentially, based on classic Wulff construction. However, here we identified that an I_h-Pt_{55} is energetically unstable. Actually, the lowest energy structure (a) is also identified as the ground state of Pt_{55} cluster by Da Silva et al.[34] using a different functional. Interestingly, we have also found a relatively ordered three-layered structure

in Fig. 1(b), which is almost as degenerate in energy as structure (a). The former is only 90 meV less stable than the latter. Detailed structural analysis reveals that structure (b) is a "double-defected three-layered-wheel" (DDTLW) configuration. By rearranging these two "defect" sites, we obtained another low-lying isomer (structure (c), denoted as DDTLW-2) with these two "defects" now lying diagonally on this cluster. The resulting energy is 0.355 eV higher than that of structure (a).

To compare Pt_{55} and Au_{55}, we have also optimized Pt_{55} with the initial coordinates taken from the lowest energy structure of Au_{55},[18] i.e., a configuration with 10 core atoms (denoted as C10-S45). This low-lying isomer of Pt_{55}, as shown in structure (d), is identified to be 0.680 eV higher in energy. We have also used the most stable Os_{55} configuration[12] as the initial structure, which leads to a structure (Fig. 1(e)) with 1.339 eV higher in energy than structure (a). These results indicate that the electronic bonding properties of Pt nanostructures are significantly different from the latest element Au and the central ones such as Os. Lastly we note that the octahedral (O_h) configuration (not shown here) is much less stable, by 6.593 eV, than structure (a), though previously O_h configuration was predicted to be the lowest energy structure for Pt_{55}.[33]

We now investigate the energetics of these low energy structures (particularly the most stable ones) when considering relativistic effects, i.e., by using the GGA+SOC calculations, since Pt is also a heavy noble element with open *d*-orbital. Furthermore, for comparisons, we have also optimized these structures by using the empirical, embedded atom model (EAM) in the LAMMPS code.[43] Our central findings are presented in Fig. 2. The relative stabilities of structure (a) and structure (b) in Fig. 1 are

strikingly tuned when the relativistic (SOC) effect are included in these calculations. Using empirical EAM potential, the structure DDTLW is now 0.312 eV higher in energy than structure in Fig. 1(a). The EAM potential is known to be generally unreliable for nanostructure predictions because it neglects the directional nature of *d*-*d* interactions and other quantum effects such as spin magnetism, orbital symmetry, and electronic shell closings.[6] As already described in Fig. 1, first-principles calculation with GGA (PW91) functional results in a significant reduction in energy from structure Fig. 1(a) to Fig. 1(b), i.e., ΔE=90 meV. Amazingly, when spin-orbital coupling is also considered (GGA+SOC), the DDTLW structure now is essentially energetically degenerate with structure (a). Actually, it is also even slightly more stable than structure Fig. 1(a), by 3 meV. Note that such a small energy difference between these two structures may be already beyond the limit of the accuracy of the present DFT calculations. However, the role of relativistic effect in shifting the relative stabilities of these two motifs are unambiguous: the SOC-induced stability change in Pt_{55} between C9-S46 and DDTLW structures is also observed in calculations with PBE functional. Furthermore, as introduced before, the relativistic effect, such as SOC, stabilizes the *s* orbitals and destabilizes the *d* orbitals, leading to the enhanced *s*-*d* hybridizations in the late TMs and reduced electron-electron repulsion in the open layered structures.[16]

Motivated by the above findings that the relativistic effects may tune the relative stability of two different Pt_{55} cluster structures, it is imperative to investigate its role in determining the magic number of Pt nanoclusters around size 55. To do this, we first optimize the most stable structures of the Pt_N clusters (N=52~61). Previously, based on

the classic Wulff construction and geometric closed-shell model, the number 55 was widely accepted as a magic number for transition metal nanoclusters. Here, by using GGA+SOC calculations, our extensive searches have found the most stable structural candidates for Pt_N clusters (N=52~61) as shown in Fig. 3. The preferred structural growth mode in this size range takes a very interesting route. The most stable Pt_{52} cluster prefers a low symmetric core-shell structure (C9-S43) over a defected-TLW-like structure, by 0.897 eV. Similarly, Pt_{53} cluster also favors a core-shell structure, denoted as C9-S44. These two structures were optimized from various arrangements for the numbers of core and shell atoms, but no layered structure with lower energy was found. Interestingly, when the cluster size increases to 54, the TLW-like structure becomes favored. An elongated-TLW configuration is found to be the most stable one for Pt_{54} cluster with each layer consisting of 18 atoms. From top view the inner three-layered core is of A-A-A stacking. The surrounding 36 atoms are arranged in an A-B-A-like stacking and form a closed hexagonal belt from the side view. This form is now slightly (~0.002 eV) more stable than the most stable amorphous core-shell structure obtained. As discussed, for Pt_{55}, the DDTLW structure is the most stable, compared with all other configurations, including those by growing one additional atom on the elongated TLW-Pt_{54} and other amorphous core-shell forms.

From size 55, larger clusters favor stable structures that can be constructed by growing additional atoms onto the DDTLW structure. For example, the lowest energy structure of Pt_{56} is a single-defected TLW configuration. As expected, Pt_{57} prefers a perfect TLW with high symmetry of D_{6h}, which is 1.812 eV more stable than the most

stable core-shell structures obtained. Even larger clusters investigated here can be optimized by growing additional atoms on the perfect TLW configuration to form another larger outer belt. Note that the large smooth facets and the sharp edges of these Pt_N nanostructures may serve as effective catalytic sites, such as for O_2 activation and H_2O splitting.[46] Here, we emphasize that the transition of structural growth mode from the amorphous core-shell to the ordered layered one occurs in the vicinity of 54 and 55, at which size these two structural motifs become essentially degenerate in energy. Specifically, this correlates with the observation that the SOC effect plays a crucial role in reversing the relative stability of these two different symmetric structures. Note also that such an energetic transition between these two structures driven by SOC effect cannot be observed for both early and central elements, as also reported in previous work[12]. Additionally, the DDTLW structure is not preferred by Pd_{55}, confirming again the importance of the relativistic effect in tuning the growth modes (from core-shell to TLW motifs) of the Pt_N clusters in the vicinity of the critical size, around 55.

To identify the magic numbers of Pt_N nanocluster around size 55, we further calculated the average binding energy per atom, $E_b(N)=-[E(Pt_N)-N\times E(Pt_{atom})]/N$, and its second-order difference, $\Delta^2E_b(N)=E_b(N+1)+E_b(N-1)-2E_b(N)$ in Fig. 4. Intriguingly, the odd number of 57 is established as the magic number, rather than the widely accepted number 55 from geometric construction. This is consistent to the perfect TLW structure in Fig. 3. Previously, we reported that for the TM_n clusters of central elements, around size 55, the magic numbers are even (such as 56) which is guided by the generalized Wulff construction principle. This principle considers the significant contribution from

edge energy minimization, so the magic size of 56 is a natural outcome of the symmetry restrictions by the corresponding even-layered fcc- or hcp-like crystal fragment configurations.[12] Here, we stress that the new odd magic number of 57, rather than 55, is also a natural outcome of an odd (rather than even) layered highly symmetric hexagonal atomic arrangement. To access the contribution of the relativistic effect in stabilizing this high symmetric magic cluster (Pt_{57}), we calculated the energy difference (ΔE) between the most stable core-shell amorphous configuration and the D_{6h} magic motif without considering the spin-orbital coupling. The calculated ΔE is only slightly reduce to 1.726 eV, from 1.812 eV obtained in the relativistic calculation, namely, the relativistic effect may merely stabilize the layered D_{6h} structure by 86 meV, which is close to the value of ~93 meV in the case of Pt_{55}. Note that for the TLW-Pt_{57}, no significant gap between the highest occupied and the lowest unoccupied molecular orbitals is observed, *i.e.*, electronic shell closure[6] is excluded.

Therefore, there must be some other mechanism taking over the relativistic effect in the structure and magicity of these layered structures. We now elucidate in more detail the underlying mechanism of the magic cluster Pt_{57} and the TLW-Pt_N motifs. Note that magic cluster Pt_{57} is of highly symmetric layered planar configuration, whereas Au_{57} and Au_{58} prefer low symmetric amorphous form that is grown on distorted I_h-Au_{55} structure.[15] To explain this contrast, we performed a calculation to relax Au_{57} cluster with the optimized D_{6h}-Pt_{57} structure as the initial configuration. Unexpectedly, we observed an amazing structural transition from the planar TLW to an interesting core-shell structure which can be viewed as a planer Au_7 core encapsulated in an elliptic D_{6h}-

Au_{50} shell whose configuration is similar to the Au_{50} cage as previously reported.[47] In this process, the two large planar surfaces of D_{6h}-Au_{57} structure significantly and smoothly arched, leading to large Au-Au bond distances along the high symmetric axis. This phenomenon indicates that the three-layered D_{6h}-Pt_{57} magic cluster may be stabilized by much stronger interlayer binding in contrast to that of Au clusters.

The above deduction has been further validated by the electronic charge-difference ($\Delta\rho$) analysis defined by $\Delta\rho=\rho(SC)-\rho(SP)$. Here, $\rho(SC)$ is obtained by a self-consistent calculation method and $\rho(SP)$ by the superposition of the atomic charge for the same structure. First, taking the optimized D_{6h}-Pt_{57} as an example, we have presented the two-dimensional $\Delta\rho$ charge contour projected onto the high symmetry plane bisecting the D_{6h}-Pt_{57} cluster as shown by the top panel in Fig. 5. Considerable charge density accumulations have been identified in the bond centers, revealing a significant level of *d*-type covalent bonding[19,20,46] of the interlayers. This argument is also further supported by the electronic density of state (DOS) analysis. In Fig. 6, we compared the DOS of the structures D_{6h}-Pt_{57} and the most stable core-shell motif C9-S48 presented in 57-(a) and 57-(b) of Fig. 3, respectively. Clearly, the strong covalent interlayer bonding in the D_{6h}-Pt_{57} results in a significant pseudo-gap around 0.5 eV below the Fermi level, simultaneously reducing the DOS as compared to the amorphous configuration. On the other hand, the sharp edge atoms of the TLW structure dominate the peaks around -0.2 eV in the DOS (see Fig. 6), which is comparable with that of the amorphous motif in the vicinity of the Fermi level, indicating no excess undesirable *d*-type dangling bonds exist on the sharp edges of the TLW as compared to C9-S48.

However, for the optimized core-shell D_{6h}-Au_{57} structure, no significant charge accumulations are observed at the interlayers, displaying a weak covalent bonding of the inner core and the surface shell. Note that although D_{6h}-Au_{57} possess weak covalent bonding between the core and shell atoms, significant charge accumulations are still observed at the Au-Au bond centers of the surface shell, which exhibits strong covalent bonding characteristic.[19,20] We have also plotted the one-dimensional $\Delta\rho$ along the six-fold axis of these structures, as presented in the lower panel of Fig. 5. A significantly stronger covalent bonding feature in Pt_{57} is further identified than that in Au_{57}, so that, correspondingly, open and planar TLW structure is preferred by the former. Our calculations show that in a four-layered Pt_{57} structure, the covalent inter-layer binding is significantly reduced as compared with TLW-Pt_{57}, due to the limited number of unpaired *d* electrons in Pt. This is another origin of the resulted odd magic number of Pt_N nanocluster around size 55, which prefers odd-layered (three-layered) high symmetric configurations.

Note also that amorphous configurations[35] for Au and Pt clusters were previously interpreted in terms of a rosette-like reconstruction of I_h structures, which essentially reduces the number of high energetic edge atoms and gives rise to local fcc (111) facet, and thus can be explained well by the recently established generalized Wulff construction principle.[12] However, here we reveal that Pt_N nanoclusters around size 55 prefer highly ordered planar configuration due to SOC, particularly the intrinsic open *d*-orbital resulted covalent bonding, as supported by the electronic structure comparison between Pt and Au performed above.

Here we emphasize that such an intriguing TLW structure and resulted magic number, as dominated by the collective effect of a relativistic effect and the open *d*-orbital enhanced covalent bonding, are also valid to the nearest neighbor element Ir. Further extensive calculations have confirmed that Ir_N cluster around size 55 also prefers the new TLW structural forms over the previously reported fcc-like crystal fragment form, by 1.989 eV, for Ir_{55}, (for more details, see also the Supplementary Materials of Ref.12), and Ir_{57} also exhibits magic cluster properties. The electronic charge contour presented in Fig. 5 verifies that Ir_{57} possesses even stronger covalent bonding characteristic as compared to its later neighbors, Pt and Au. Thus, we can conclude that, to stabilize these TLW structures, the contribution from the covalent bonding due to the intrinsic open *d*-orbital in Ir, Pt and Au is qualitatively of the following sequence: Ir > Pt > Au, though the enhanced covalent bonding due to a pure relativistic effect is completely reversed: Ir < Pt < Au.[28] In conclusion, the magicity of highly symmetric D_{6h}-Pt_{57} nanocluster is facilitated not only by the SOC effects which effectively enhance the *s*-*d* hybridization by the Fermi level, but also by the intrinsic open *d*-orbital which significantly enhance the covalent bonding of the inter-layers.

To the end, we emphasize that for the cases of Pt_N and Ir_N around size 55, the GWCP still plays an important role in determining their preferred structures, as manifested by the enlarged surface areas and reduced edge length.[12] Note that for Pt_{57}, four-layered planar configurations are found to be dramatically unstable, due to significantly enlarged areas of high energy facets and particularly the increased number of low-coordinated edge atoms. Importantly, moving towards the central element Os with more

unpaired *d* electrons as compared to Ir and Pt, the GWCP mechanism dominates and the present TLW forms are significantly less stable than those structures predicted by GWCP[12], due to the critically undesirable *d*-type dangling bonds[12] located on the sharp edges of TLW structure, as manifested by the enhanced DOS peaks by the Fermi level, see also Fig. 6. Additionally, we have summarized the four established mechanisms in determining the atomic stacking rule and magic numbers of a given elemental nanocluster around the size 55 in a "magicity table", to schematically highlight the position- or electronic configuration-dependent mechanisms. As have been discussed, these four representative mechanisms are atomic shell closure for inert gas, electronic shell closure for simple metal (both atomic and electronic shell closure for fullerene), generalized Wulff construction principle for transition metal, and synergetic effects (including SOC) for heavy noble elements, such as Au, respectively, Fig. 7. To do this, we have comparatively presented the geometric structures of the representative magic nanoclusters around size 55, such as Na_{58}, Y_{55}[12], Cu_{55}[12], Ag_{55}[12,18], Ar_{55}[5], Ru_{56}[12], Ag_{58}[12,18], Pt_{57}, Au_{58}[15], and C_{60}, of which the magic mechanisms are indicated by different models. For example, atomic close-shelled magic cluster Ag_{55} is presented by a space-filling model, and the magic clusters of Ag_{58}, Au_{58}, and C_{60} of both atomic and electronic shell closures are shown in ball-and-stick structure embedded in electronic charge, respectively. We wish this magic table is highly instructive for readers to readily catch the characteristic mechanism for a given elemental nanocluster.

Before closing, we emphasize that the present findings obtained by theoretical calculations are based on the gas phase nanoclusters, and wish these interesting results

may motivate future experimental efforts. Additionally, clusters deposited on surfaces naturally lead to variations of the cluster-surface contact and bindings, charge transfer may also occur between the clusters and substrate, thereby leading their structures, magicity,[48] and catalysis to change, which are of our great interest in future investigations.

IV. Conclusions

Previously, electronic/geometric closed-shell models and generalized Wulff construction principle have been established to predict the atomic stacking rule and magic numbers of early/late and central elemental TM nanoclusters, respectively. However, for heavy noble elemental nanoclusters, such as Pt_N and Ir_N, it is difficult to predict their atomic stacking rule and magic numbers using these established principles, because these elements lie on the boundaries of different domains of the periodic table that are governed by different principles. In this paper, by means of first-principles calculations, we have specifically identified that Pt_N nanoclusters around size 55 prefer an intriguing three-layered structural growth mode, a result of the synergetic effect from the generalized Wulff construction principle, relativistic effect, particularly the open-*d*-orbital enhanced covalent bonding. Correspondingly, the magic cluster of Pt_N around size 55 is unexpectedly shifted from the widely accepted number 55 to 57, leading to a three-layered-wheel (TLW) structure with D_{6h} symmetry. The present findings are found to be valid up to the case of Ir. (note: these interesting results deserve of further experimental examinations, such as photoelectron spectra analysis). The contrast atomic stacking form and magic numbers around 55 between Pt_N (Ir_N) and Au_N clusters

are mainly due to the relatively stronger covalent bonding stemmed from the open-shelled *d* orbital in the former case, as opposed to the closed-shell of the latter, although the relativistic effect is weaker for the former. The present findings are important supplementary of the recently established GWCP which is expected to play an instrumental role in future design of novel metal based nanostructures with desirable functionalities for potential applications such as in nanocatalysis.

This work was supported by the Natural Science Foundation of China (11074223 and 11034006) and the US National Science Foundation (CMMI 0900027, CMMI 1300223, and DMR 0906025).

a) sflizzu@zzu.edu.cn

b) zhangzy@ustc.edu.cn

c) ygao7@utk.edu

References:

[1]W. P. Halperin, Rev. Mod. Phys. **58**, 533-606 (1986).

[2]D. I. Gittins, D. Bethell, D. J. Schiffrin, and R. J. Nichols, Nature **408**, 67-69 (2000).

[3]H. G. Boyen, G. Kastle, F. Weigl, B. Koslowski, C. Dietrich, P. Ziemann, J. P. Spatz, S. Riethmuller, C. Hartmann, M. Moller *et al.*, Science **297**, 1533-1536 (2002).

[4]A. A. Herzing, C. J. Kiely, A. F. Carley, P. Landon, and G. J. Hutchings, Science **321**, 1331-1335 (2008).

[5]O. Echt, K. Sattler, and E. Recknagel, Phys. Rev. Lett. **47**, 1121-1124 (1981).

[6]W. D. Knight, K. Clemenger, W. A. de Heer, W. A. Saunders, M. Y. Chou, and M. L. Cohen, Phys. Rev. Lett. **52**, 2141-2143 (1984).

[7]H. W. Kroto, J. R. Heath, S. C. Obrien, R. F. Curl, and R. E. Smalley, Nature **318**, 162-163 (1985).

[8]X. Li, A. Grubisic, S. T. Stokes, J. Cordes, G. F. Ganteför, K. H. Bowen, B. Kiran, M. Willis, P. Jena, R. Burgert *et al.*, Science **315**, 356-358 (2007).

[9]A. F. Hebard, M. J. Rosseinsky, R. C. Haddon, D. W. Murphy, S. H. Glarum, T. T. M. Palstra, A. P. Ramirez, and A. R. Kortan, Nature **350**, 600-601 (1991).

[10]M. Yoon, S. Yang, C. Hicke, E. Wang, D. Geohegan, and Z. Zhang, Phys. Rev. Lett. **100**, 206806 (2008).

[11]S. N. Khanna, and P. Jena, Phys. Rev. Lett. **69**, 1664-1667 (1992).

[12]S. F. Li, X. J. Zhao, X. S. Xu, Y. F. Gao, and Z. Zhang, Phys. Rev. Lett. **111**, 115501 (2013).

[13]T. Rapps, R. Ahlrichs, E. Waldt, M. M. Kappes, and D. Schooss, Angew. Chem. Int. Ed. **52**, 6102-6105 (2013).

[14]S. Yin, X. Xu, A. Liang, J. Bowlan, R. Moro, and W. de Heer, J. Supercond. Nov. Magn. **21**, 265-269 (2008).

[15]W. Huang, M. Ji, C.-D. Dong, X. Gu, L.-M. Wang, X. G. Gong, and L.-S. Wang, ACS Nano

2, 897-904 (2008).

[16]C. M. Chang, and M. Y. Chou, Phys. Rev. Lett. **93**, 133401 (2004).

[17]H. Häkkinen, M. Moseler, and U. Landman, Phys. Rev. Lett. **89**, 033401 (2002).

[18]H. Häkkinen, M. Moseler, O. Kostko, N. Morgner, M. A. Hoffmann, and B. v. Issendorff, Phys. Rev. Lett. **93**, 093401 (2004).

[19]L.-S. Wang, Phys. Chem. Chem. Phys. **12**, 8694-8705 (2010).

[20]X.-B. Wang, Y.-L. Wang, J. Yang, X.-P. Xing, J. Li, and L.-S. Wang, J. Am. Chem. Soc. **131**, 16368-16370 (2009).

[21]S. Bulusu, X. Li, L.-S. Wang, and X. C. Zeng, P. Natl. Acad. Sci. **103**, 8326-8330 (2006).

[22]M. Valden, X. Lai, and D. W. Goodman, Science **281**, 1647-1650 (1998).

[23]T. Bunluesin, R. J. Gorte, and G. W. Graham, Appl. Catal. B: Environ. **15**, 107-114 (1998).

[24]K. M. Bratlie, H. Lee, K. Komvopoulos, P. Yang, and G. A. Somorjai, Nano Lett. **7**, 3097-3101 (2007).

[25]Y. Mu, H. Liang, J. Hu, L. Jiang, and L. Wan, J. Phys. Chem. B **109**, 22212-22216 (2005).

[26]M. L. Anderson, R. M. Stroud, and D. R. Rolison, Nano Lett. **2**, 235-240 (2002).

[27]K. Vinodgopal, M. Haria, D. Meisel, and P. Kamat, Nano Lett. **4**, 415-418 (2004).

[28]P. Pyykko, and J. P. Desclaux, Acc. Chem. Res. **12**, 276-281 (1979).

[29]Y. Sun, M. Zhang, and R. Fournier, Phys. Rev. B **77**, 075435 (2008).

[30]M. Zhang, and R. Fournier, Phys. Rev. A **79**, 043203 (2009).

[31]F. Baletto, R. Ferrando, A. Fortunelli, F. Montalenti, and C. Mottet, J. Chem. Phys. **116**, 3856-3863 (2002).

[32]E. Aprà, and A. Fortunelli, J. Phys. Chem. A **107**, 2934-2942 (2003).

[33]V. Kumar, and Y. Kawazoe, Phys. Rev. B **77**, 205418 (2008).

[34]J. L. F. Da Silva, H. G. Kim, M. J. Piotrowski, M. J. Prieto, and G. Tremiliosi-Filho, Phys. Rev. B **82**, 205424 (2010).

[35]E. Aprà, F. Baletto, R. Ferrando, and A. Fortunelli, Phys. Rev. Lett. **93**, 065502 (2004).

[36]P. Hohenberg, and W. Kohn, Phys. Rev. **136**, B864-B871 (1964).

[37]J. P. Perdew, J. A. Chevary, S. H. Vosko, K. A. Jackson, M. R. Pederson, D. J. Singh, and C. Fiolhais, Phys. Rev. B **46**, 6671-6687 (1992).

[38]G. Kresse, and J. Hafner, Phys. Rev. B **49**, 14251-14269 (1994).

[39]P. E. Blöchl, Phys. Rev. B **50**, 17953-17979 (1994).

[40]J. C. Fabbi, J. D. Langenberg, Q. D. Costello, M. D. Morse, and L. Karlsson, J. Chem. Phys. **115**, 7543-7549 (2001).

[41]M. B. Airola, and M. D. Morse, J. Chem. Phys. **116**, 1313-1317 (2002).

[42]C. Kittel. *Introduction to Solid State Physics*. (Wiley, New York, 1976).

[43]S. Plimpton, J. Comput. Phys. **117**, 1-19 (1995).

[44]Y. Wang, J. Lv, L. Zhu, and Y. Ma, Phys. Rev. B **82**, 094116 (2010).

[45]Y. Wang, J. Lv, L. Zhu, and Y. Ma, Comput. Phys. Commun. **183**, 2063-2070 (2012).

[46]S. F. Li, H. Li, X. Xue, Y. Jia, Z. X. Guo, Z. Zhang, and X. G. Gong, Phys. Rev. B **82**, 035443 (2010).

[47]D. Tian, J. Zhao, B. Wang, and R. B. King, J. Phys. Chem. A **111**, 411-414 (2006).

[48]H. Hakkinen, and M. Manninen, Phys. Rev. Lett. **76**, 1599-1602 (1996).

Figure Captions:

FIG. 1 (color online). Geometric structures and relative energies of the 6 representative low energy configurations of Pt_{55} obtained by GGA calculations. The relative energies in (a)-(f) are measured from that of the C9-S46 structure in (a), given by $\Delta E = E(Pt_{55}) - E(Pt_{55}(C9\text{-}S46))$.

FIG. 2 (color online). The relative energies of Pt_{55} with the double-defected three-layered wheel (DDTLW) structure as compared to that of the core-shell configuration of C9-S46, given by E(DDTLW)-E(C9-S46), against different functionals or calculation methods.

FIG. 3 (color online). The optimized minimum energy structures of Pt_N cluster around size 55 (N=52~61), and by calculations considering spin-orbital coupling with PW91 functional. For Pt_{57} cluster, 57-(a) represents the most stable configuration, and the first low-lying amorphous core-shell configuration (C9-S48) is also shown in 57-(b), respectively.

FIG.4 (color online). Average binding energy per atom, $E_b(N) = -[E(Pt_N) - N \times E(Pt_{atom})]/N$, and its second-order finite difference, $\Delta^2 E_b(N) = E_b(N+1) + E_b(N-1) - 2E_b(N)$, for different Pt_N clusters presented in Fig. 3. The data points marked by circles are for the binding energies, $E_b(N)$, and stars represent the second-order derivatives, $\Delta^2 E_b(N)$.

FIG. 5 (color online). The two-dimensional (top panel) and one-dimensional (bottom panel) electronic charge-difference ($\Delta\rho$) plots for Ir_{57}, Pt_{57}, and Au_{57}, with $\Delta\rho=\rho(SC)-\rho(SP)$. Here, $\rho(SC)$ is obtained by a self-consistent GGA+SOC calculation method and $\rho(SP)$ by the superposition of the atomic charge for the same structure. The one-dimensional $\Delta\rho$ is obtained along the axis of the bonds of the interlayers for different systems, and the bond lengths are shown in normalized scale. See the corresponding labels of "A, B, C" in these two panels.

FIG. 6 (color online). Electronic density of states (DOS) of Pt_{57} clusters. Filled data represent the DOS of the high symmetric TLW-Pt_{57} while the red lines represent the DOS of the amorphous core shell C9-S48 structures, respectively.

FIG. 7 (color online). Schematic "magicity table" of the four mechanisms established in determining the atomic stacking rule and magic numbers of nanoclusters, including atomic shell closure for inert gas, electronic shell closure for simple metal, generalized Wulff construction principle for transition metal, and relativistic effects for heavy noble elements, respectively. The relative importance of a given mechanism is marked by the color shade. Correspondingly, we have also schematically presented the geometric structures of the representative elemental magic-sized nanoclusters around size 55, such as Na_{58}, Y_{55}, Cu_{55}, Ag_{55}, Ar_{55}, Ru_{56}, Ag_{58}, Pt_{57}, Au_{58}, and C_{60}, respectively. Refer to text for detailed interpretations of these structures.

Figures:

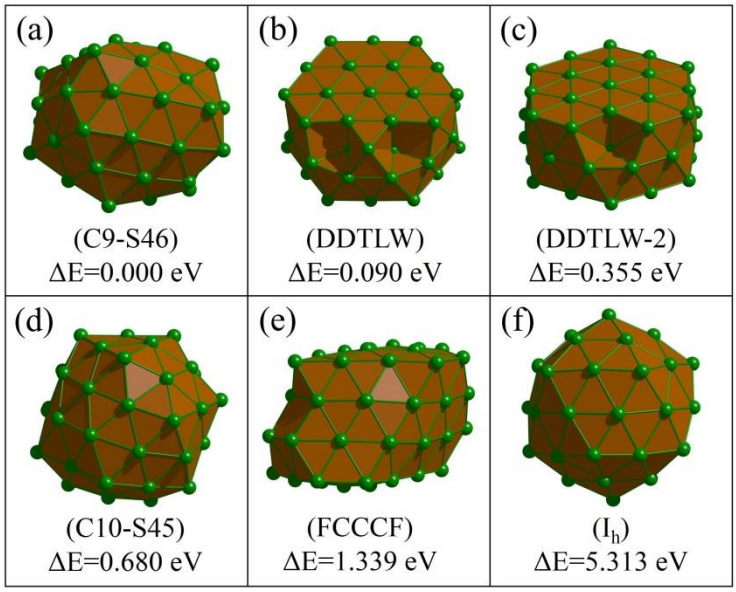

Fig. 1

(Zhao, *et al.*, to JCP)

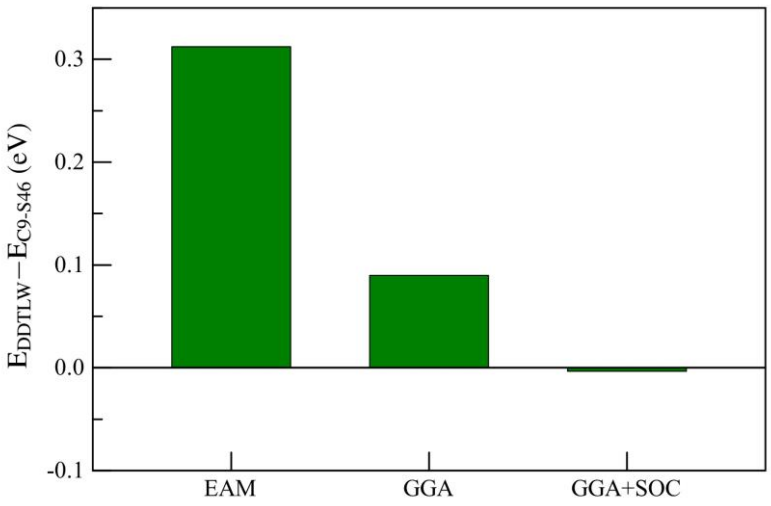

Fig. 2

(Zhao, *et al*., to JCP)

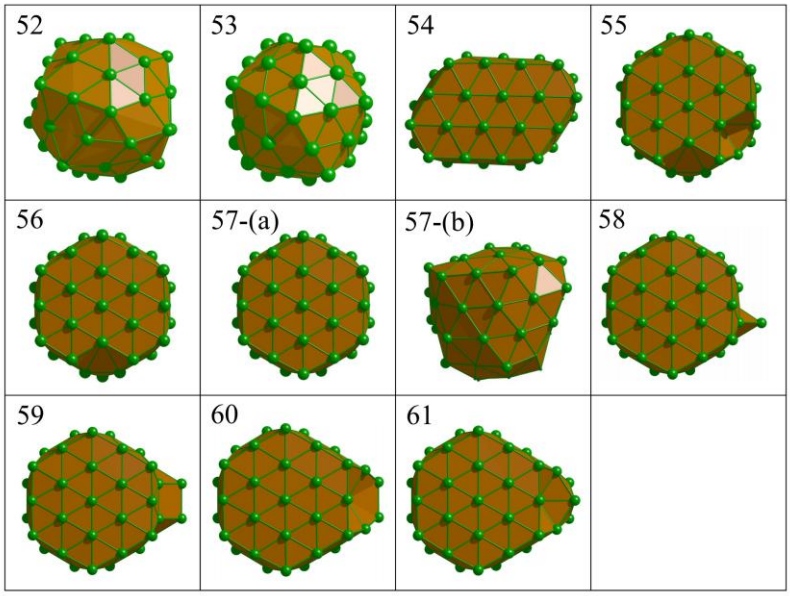

Fig. 3

(Zhao, *et al.*, to JCP)

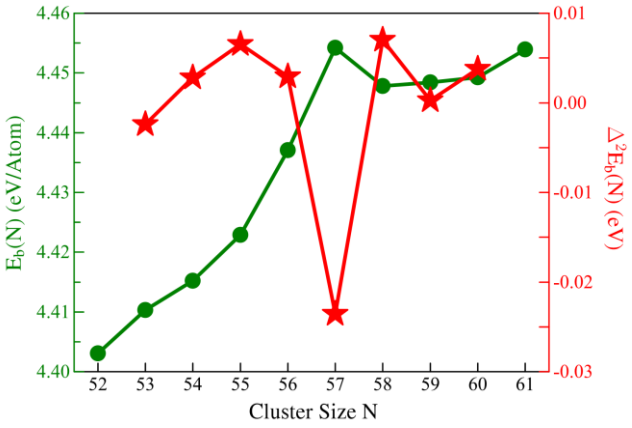

Fig. 4

(Zhao, *et al*., to JCP)

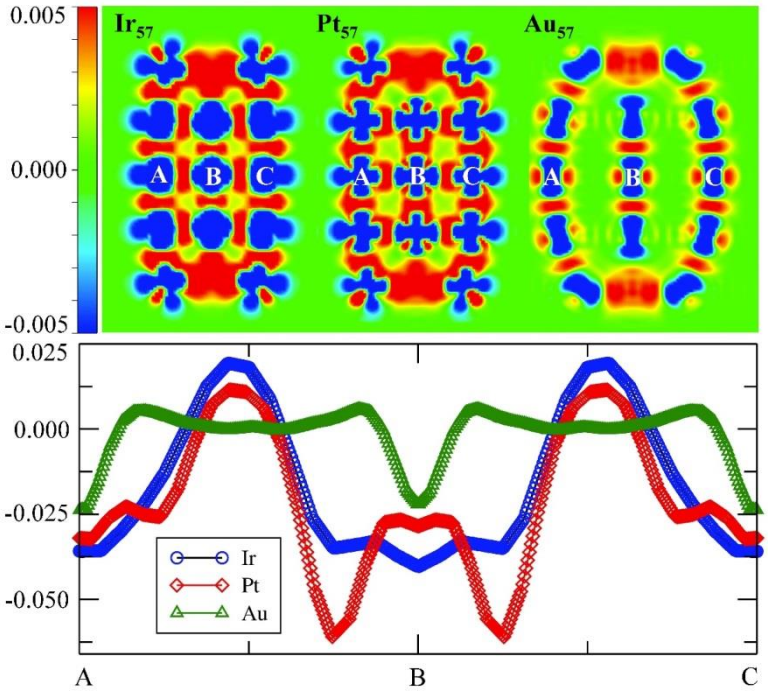

Fig.5

(Zhao, *et al*., to JCP)

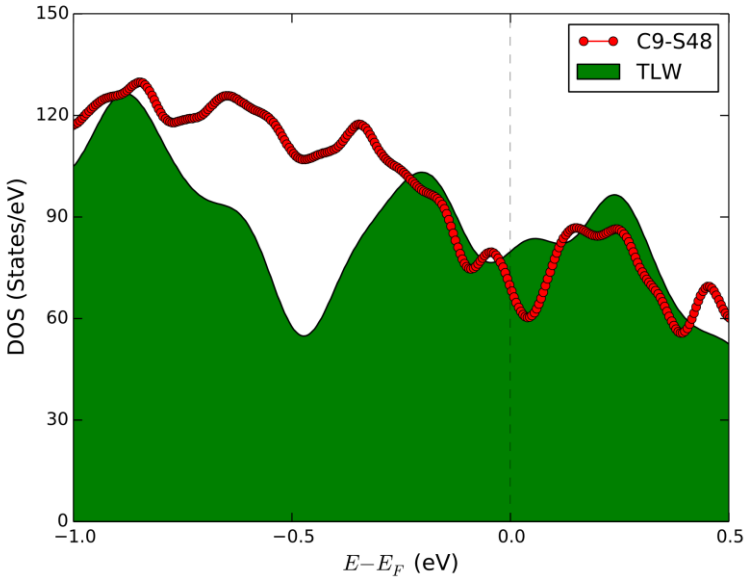

Fig.6

(Zhao, *et al*., to JCP)

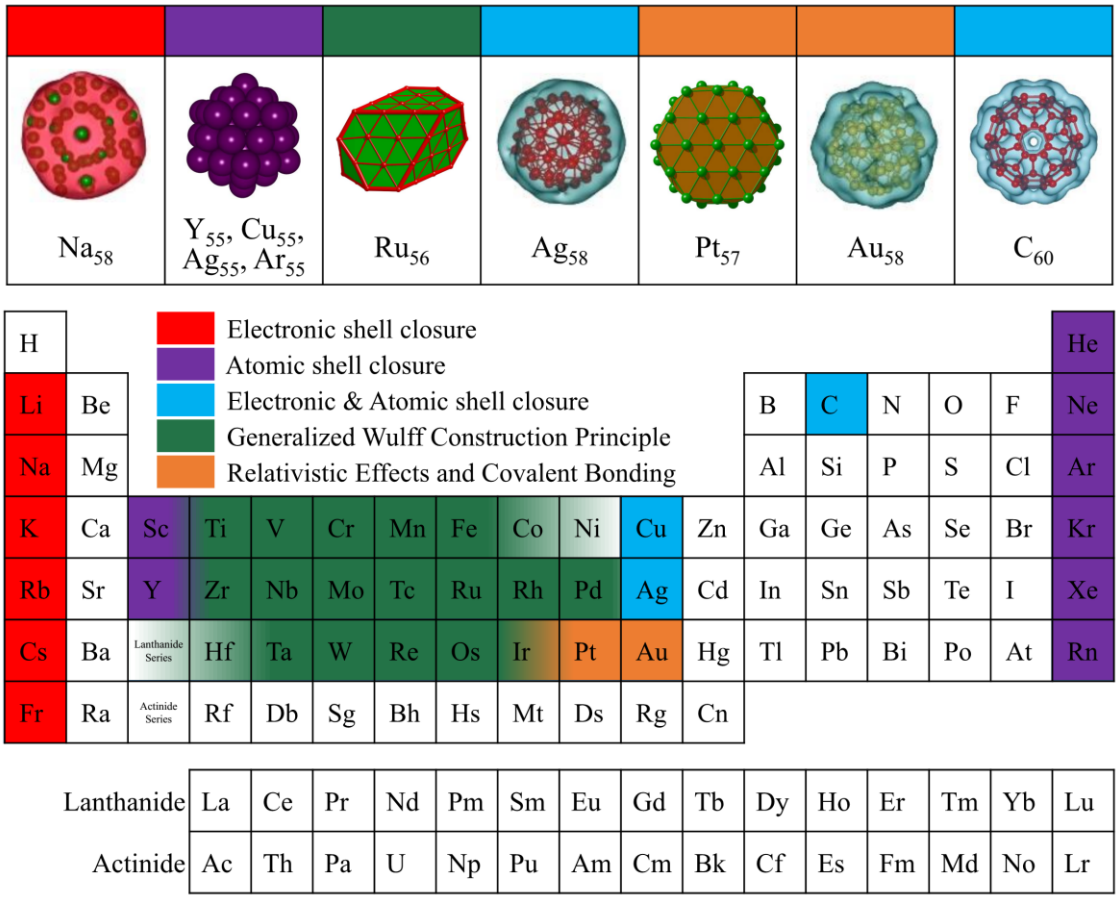

Fig.7

(Zhao, *et al.*, to JCP)